Geomechanics and Engineering, *Vol. 38, No. 2 (2024) 157-164*
https://doi.org/10.12989/gae.2024.38.2.157

The behaviors of a Korean weathered soil under monotonic loadings

Sangseom Jeong[1a], Junyoung Ko[2b], Sumin Song*[1] and Jaehong Kim[3c]

[1]*School of Civil and Environmental Engineering, Yonsei University, 50 Yonsei-ro, Seodaemun-gu, Seoul 03722, Republic of Korea*
[2]*Department of Civil Engineering, Chungnam National University, 99 Daehak-ro, Yuseong-gu, Daejeon 34134, Republic of Korea*
[3]*Department of Civil Engineering, Dongshin University, 67 Dongshindae-gil, Naju-si, 58245, Republic of Korea*

(*Received February 2, 2023, Revised May 20, 2024, Accepted July 6, 2024*)

Abstract. This paper describes the general trends of the stress-strain behavior of Korean weathered soil prior to failure and behavior at failure under triaxial loading. The isotropically consolidated samples were tested in a testing device under monotonic undrained loading. Relative density, effective mean pressure and fine content were the factors varied in the experimental investigation. The test results were analyzed and their behaviors were interpreted within the framework of plasticity constitutive model for a weathered Korean silty sand. Possible physical bases for the proposed forms are discussed. Validation of the applied model using the laboratory results is also given.

Keywords: constitutive model; monotonic undrained loading; silty sand; triaxial testing; weathered soil

1. Introduction

Two-thirds of the total land area of Korean peninsula are composed of weathered soils formed from the in-situ weathering of granite and gneiss, acting to depths lesser than 40m. Many weathered soils can be classified as SW or SM according to the Unified Soil Classification System (USCS). These soils consist mainly of completely weathered material with a shallow cover of residual soil and have the special characteristics when water saturated: they significantly lose their shear strength and unconfined compressive strength, they are fragile and their grains break down in water as observed in grain size analysis (Lee and de Freitas 1989, Aziz 2020, Gu *et al.* 2022). Thus, they show shear behavior which are intermediate to the behavior of plastic soils and non-plastic soils. They do not necessarily achieve a peak deviator stress and show both contracting and dilatancy. Conventional undrained triaxial tests done by (Abdul-Khader and Jeong 2021) on non-plastic silty sands shows that they do even above 20 % axial strain they do not show any peak deviator stress. This is due to the shear induced hardening happening in the soil. Initially the pore pressure increases until the stress path reaches a certain point (i.e., phase transformation line). After this there is dilatant behavior shown with increasing deviator stress. This is also shown in offshore silts (Fleming and Duncan 1990), low plasticity clay (Peters 1988) and clayey sand (Georgiannou *et al.* 1990, Shin and Jeong 1999).

Although advanced models like SANISAND (Dafalias and Manzari 2004), PM4Sand (Ziotopoulou and Boulanger, 2013), PM4silt, UBCSAND (Beaty and Byrne 1998, Puebla *et al.* 1997), and Nor-sand (Jefferies 1993) may be used for non-plastic soils, they tend to use too many parameters which tend to add complexity to the problem. These models have been developed to take into account the cyclic behavior and stress history. Consequently, these such advanced models are not necessarily required to compute the undrained shear behavior of such soil (Lin *et al.* 2018).

In contrast the modified Cam clay model for plastic soils (Roscoe and Burland 1968, Wood 1990, Silvestri and Abou-Samra 2012, Li and Zoua 2019) uses only 5 soil parameters and has to keep track of limited state parameters. This has been widely adopted for modeling clayey soils. In the present paper a model developed similar in concept to the modified Cam clay model is used. The yield surfaces and plastic potential for this model were proposed by Yu and Axelsson 1992. The simplicity of the modified Cam clay model and the ease of obtaining the parameter from simple laboratory tests are the main driving force to adopt such a method.

The main additions in this model are that instead of an elliptical yield surface, an ellipse aspect ratio parameter is introduced to better predict the soil behavior. In addition, deviator shear hardening is introduced to account for the post phase transformation hardening shown by the soil. The model was then calibrated for the results of the undrained behavior of Korean weathered silty sand (SM soil) made under different sample preparation methods at different densities and effective stress. Therefore, in this study, the shear behavior of the most widely distributed weathered soil was confirmed through an experiment, and the behavior was predicted through a constitutive equation model suitable for the weathered silty sand soil.

*Corresponding author, Ph.D., Post-doctoral
E-mail: ssm9780@yonsei.ac.kr
[a]Professor
E-mail: soj9081@yonsei.ac.kr
[b]Associate Professor
E-mail: jyko@cnu.ac.kr
[c]Professor
E-mail: woghd@dsu.ac.kr

ISSN: 2005-307X (Print), 2092-6219 (Online)

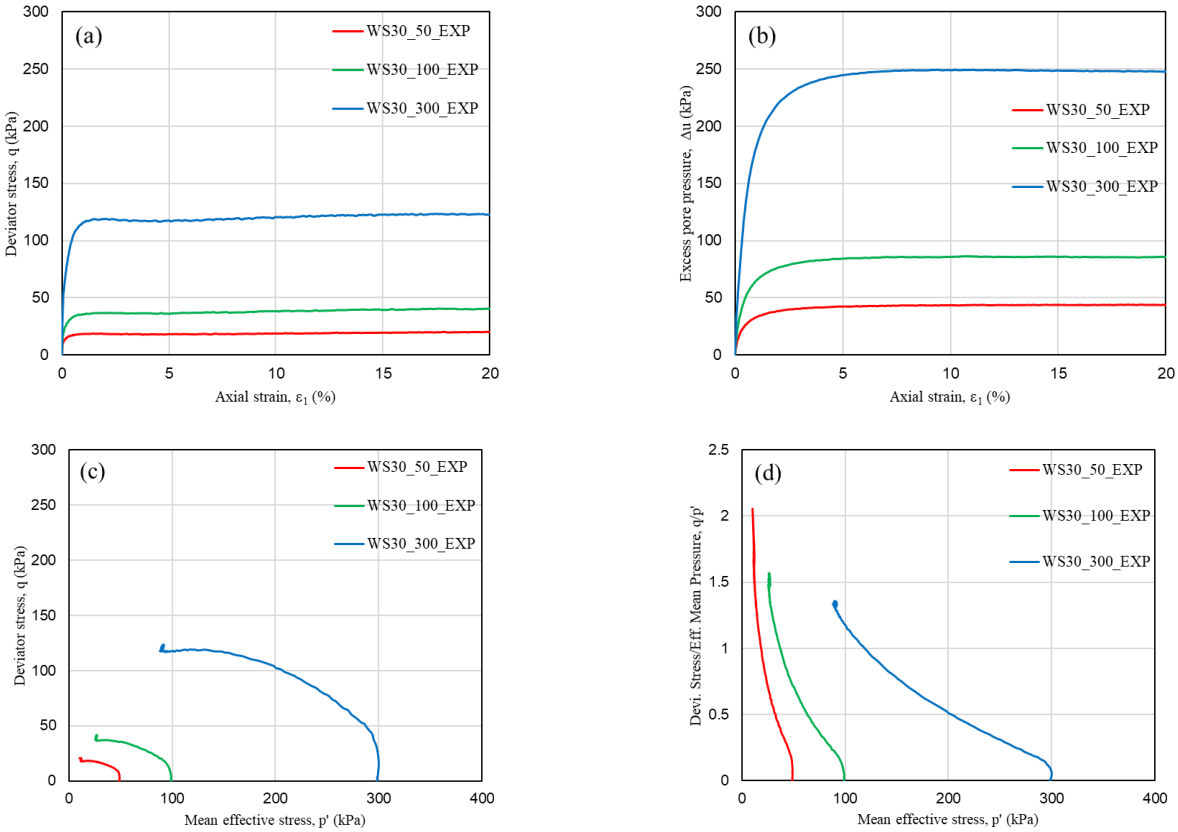

Fig. 1 Experimental values of 30% relative density

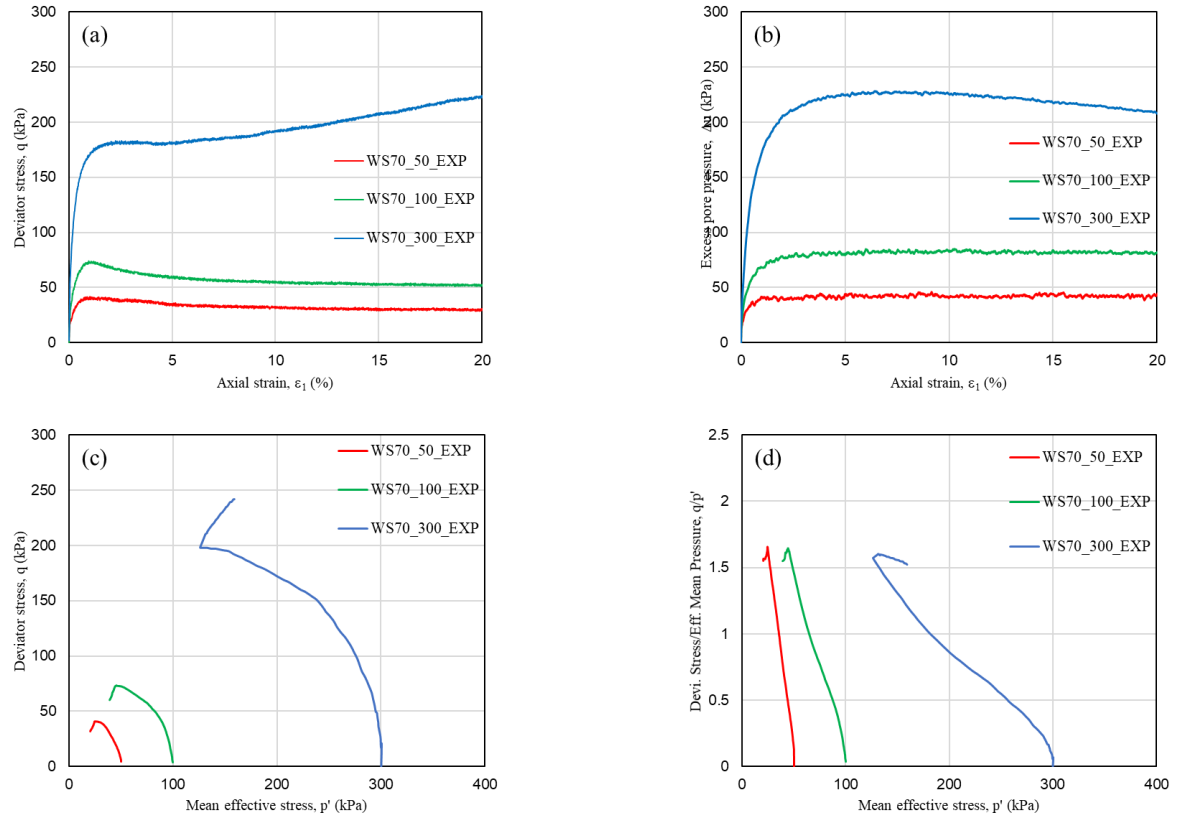

Fig. 2 Experimental values of 70% relative density

Table 1 Index properties of weathered soil

Liquid limit, LL (%)	44.4
Plastic limit, PL (%)	28.29
Plasticity index, PI (%)	16.11
$\gamma_{d\ max}$ (g/cm^3)	1.84
$\gamma_{d\ min}$ (g/cm^3)	1.12
USCS classification	Sandy silt (SM)
Specific gravity of solids, G_s	2.71

2. Experimental approach

2.1 Remodeled soil samples

The soil used in this study is non-plastic and has about 50% sand and 33% silt. It can be classified as SM according to the Unified Soil Classification System. The pertinent information regarding the physical properties of the soil is given in Table 1.

The sample preparation methods used in the remolded samples include the dry deposition method, moist temping method, and air injection method to obtain uniform sample. In this study, six undrained triaxial tests (Table 2) were performed, and the identical moist temping method was employed in all the tests.

Triaxial samples were prepared from oven-dried soil directly on the triaxial pedestal. The test soil samples were modeled in a frame of height (140mm) and diameter (70mm). There are two methods for sample preparation in this study; i) A method of dry pouring (DP) was chosen for preparing samples of relative density of 70%, and ii) The soil samples with relative density of 30 % were modeled by moist tamping (MT) of soil. This is because the soil sample with a relative density of 70 % can be self-standing, but a relative density of 30 % is not. However, the moist temping methods have limitations for making homogeneous soil sample conditions. In the moist temping method when compacting a sample, the next layer is formed after compacting the height of each layer to be constant. However, in the case of remolding in this manner, the density tends to increase toward the lower layer of the sample. To improve this, in this study, the 10-layer under-compacting method was applied so that an equal amount of soil could be reformed by calculating the volume of the specimen according to the relative density. The test sample was prepared by preparing a wet sample with a water content of about 5%, sealing it for 24 hours or more, evenly dispersing the moisture.

The sample thus prepared was then held under suction of -10 kPa and the triaxial cell was sealed and filled with water. An initial cell pressure of 20 kPa was then applied while CO_2 was flushed from the bottom of the sample at 15 kPa pressure for 20 minutes, followed by flushing with de-aired water. Figs. 1(a)-1(c) shows the steps during the preparation of the sample for triaxial testing. Subsequent to this the sample was subjected to backpressure saturation till Skempton's pore pressure coefficient (*B)* of at least 0.95 was achieved. After this, the sample was subjected to isotropic consolidation by increasing the cell pressure while maintaining constant backpressure. Subsequently, the sample was subjected to undrained shear loading.

Table 2 Summary of tests performed under undrained loading

Test	Unit weight after consolidation (kN/m^3)	Relative density after consolidation (%)	Mean effective stress p'_0 (kPa)
*WS30_50_EXP	12.3	28.5	49.2
WS30_100_EXP	12.3	28.2	99.0
WS30_300_EXP	12.5	31.0	298.0
*WS70_50_EXP	15.5	69.8	50
WS70_100_EXP	15.6	70.8	100
WS70_300_EXP	15.7	72.3	300

*WS30_50_EXP: Test sample with loose (30%) density and initial mean pressure 50kPa.
*WS70_50_EXP: Test sample with dense (70%) density and initial mean pressure 50kPa.

In this study, triaxial compression test devices of Geocomp's Load Trac-II (Geocomp Corp. 2013) were used. The Load Trac-II is a form in which the load plate at the lower part of the sample moves up and down to load the load, and the load can be measured through the measurement sensor located on the upper part. The sample was trimmed to approximately 140 mm; in height and 70mm in diameter. Porous stones were placed on the top and the bottom of the sample, and the membrane was pulled up around the top cap and clamped with O-rings. After assembling the triaxial compression cell, supply distilled water inside the cell to completely fill the inner cell, and both the back and cell pressure are generally increased for the full saturation of sample. When the sample was completely filled with distilled water, the difference between the confining pressure (cell pressure) and the back pressure (sample pressure) was set to 5 kPa, and the back pressure was increased by 20 kPa at each stage, up to 300 kPa over 2 to 3 hours. The B-value was measured at each back pressure step, and if the value was over 0.95, it was considered completely saturated. Once the saturation was completed in this way, an effective confining pressure of 50 to 300 kPa was created, and consolidation was performed until the pore water pressure was completely dissipated. Through several stages of loading increments, the desired effective confining pressure is achieved. All samples were isotropically normally consolidated with 400 kPa of effective mean confining pressure and each sample is unloaded to 300, 100, 50 kPa, respectively. Then the undrained shear tests were performed with different confining pressures. The undrained compression test was performed on all samples at a rate of 0.1%/min as a method of controlling the strain during shearing. Tests were performed on the automated triaxial testing system which is capable of conducting tests with controlled strain rate of loading for different types of prescribed stress paths of undrained conditions. The system uses two feedback control

loops, one for the axial actuator and the other for the lateral actuator. Under software control the two loops can work individually or synchronously.

2.2 Test results

A series of CIU triaxial tests were performed: they were strain-controlled triaxial compression tests under undrained conditions. These tests were performed to obtain the general behavior of weathered soil (SM), to calibrate, and to validate the proposed model for weathered soil.

Typical results of the effective stress paths in the p' - q space for test soil (SM) with 30% and 70% densities are shown in Figs. 1 and 2.

These results are in the following:

(1) There exist failure line $q/p' = M_c$ that is independent of the relative density, and confining pressure for the tested range (p_0_$\leq$ 300 kPa).
The typical stress strain response includes an initial portion of high stiffness, followed by a portion with a gradual increase in the stress values. There is no constant stress attained even though the excess pore pressure ratio stabilizes. This is typical for all the six tests.

(2) The stress path shows an initial elliptical path similar to the ones shown by fine grained soils and eventually reaching the critical state line (CSL) and then moves along the CSL. In addition, looking at the p' - q/p' graph, in the case of loose soil, it tends to approach the M (M = 1.5) value during compression, and in the case of dense soil, it tends to approach the M value after dilation occurs.

(3) The behavior is similar to the behavior shown by non-plastic sands, but the shear hardening is in a much lower scale. Comparing the two tests at the same effective stresses shows that both the stress path shows an elliptical initial stress path, difference being higher density tests following an ellipse with lower aspect ratio and showing slightly higher dilatant behavior.

3. Plasticity formulation

3.1 Yield criterion and plastic potential

The developed soil model, as shown in Fig. 3 is defined using a state surface which has to distinct yield surface f and plastic potential g segments for contractions portion ($\eta = \frac{q}{p'} < M$) given by (Yu and Axelsson 1992)

$$f_1 = g_1 = \frac{1}{\beta^2}\left(\frac{p'}{p'_m} - 1\right)^2 + \left(\frac{q}{Mp'_m}\right)^2 - 1 = 0 \quad (1)$$

and for dilatancy portion ($\eta = \frac{q}{p'} \geq M$) given by

$$f_2 = \frac{q}{Mp'} + \ln\left(\frac{p'}{p'_m}\right) - 1 = 0 \quad (2)$$

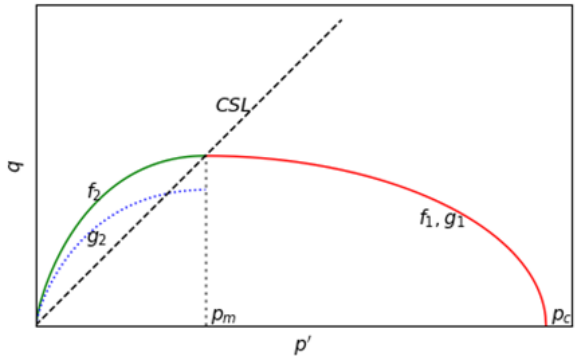

Fig. 3 Yield functions f_1, f_2 and potential function g_1 and g_2 on the stress space

$$g_2 = \frac{q}{Np'} + \ln\left(\frac{p'}{p'_m}\right) - 1 = 0 \quad (3)$$

where M is the slope of the CSL and N defines the plastic function g_2.

β governs the yield surface ellipse aspect ratio given by

$$\beta = \frac{p'_c}{p'_m} - 1 \quad (4)$$

where p'_c is the size of the yield function and p'_m is the mean effective stress at intersection of yield function with CSL $q = Mp'$ as shown in Fig. 3.

It is to be noted that yield function f_1 and f_2 are continuous and differentiable at p'_m andplastic potential function has the same slope when approaching p'_m from either side. An elliptical cap surface and associated flow rule is used in contractions portion while a logarithmic surface and non-associated flow rule is used in the dilatancy portion.

3.2 Flow rule and hardening function

The flow rule is given by

$$d\varepsilon_v^p = \Lambda \frac{\partial g}{\partial p'} \quad (5)$$

$$d\varepsilon_q^p = \Lambda \frac{\partial g}{\partial q} \quad (6)$$

where $d\varepsilon_v^p$ and $d\varepsilon_q^p$ are the plastic volumetric strain and plastic shear strain and Λ is a hardening parameter.

The strain hardening rule is given by (Nova and Wood 1979)

$$\frac{\partial p'_m}{\partial \varepsilon_v^p} = \frac{1}{\lambda - \kappa} p'_m \quad (7)$$

and

$$\frac{\partial p'_m}{\partial \varepsilon_q^p} = \frac{D}{\lambda - \kappa} p'_m \quad (8)$$

where D is a dilatancy parameter, λ is the slope of the normal compression line and κ is the slope of the recompression line.

Table 3 Plasticity properties of test soil

Properties	λ	κ	M	D	β	v_0	p_o' (kPa)
WS30_50_PRD*	0.107	0.006	1.5	0.05	3.3	2.309	50
WS30_100_PRD						2.291	100
WS30_300_PRD						2.116	300
WS70_50_PRD**					1.2	1.746	50
WS70_100_PRD						1.746	100
WS70_300_PRD						1.746	300

* Predicted with loose (30%) density and initial mean pressure 50 kPa
** Predicted with dense (70%) density and initial mean pressure 50 kPa

Integration of these equations yield

$$p_m' = p_{m0}' \exp\left(\frac{\varepsilon_v^p + D\varepsilon_q^p}{\lambda - \kappa}\right) \frac{\partial p_m'}{\partial \varepsilon_q^p} = \frac{D}{\lambda - \kappa} p_m' \tag{9}$$

where p_{m0}' is the initial value of p_m'.

The stress strain relation can be derived for this as

$$\begin{Bmatrix} dp' \\ dq \end{Bmatrix} = \begin{bmatrix} K\left(1 - \frac{K}{\bar{H}}\frac{\partial f}{\partial p'}\frac{\partial g}{\partial p'}\right) & -\frac{3KG}{\bar{H}}\frac{\partial f}{\partial q}\frac{\partial g}{\partial p'} \\ -\frac{3KG}{\bar{H}}\frac{\partial f}{\partial p'}\frac{\partial g}{\partial q} & 3G\left(1 - \frac{3G}{\bar{H}}\frac{\partial f}{\partial q}\frac{\partial g}{\partial q}\right) \end{bmatrix} \begin{Bmatrix} d\varepsilon_v \\ d\varepsilon_q \end{Bmatrix} \tag{10}$$

where

$$\bar{H} = H + K\frac{\partial g}{\partial p'}\frac{\partial f}{\partial p'} + 3G\frac{\partial g}{\partial q}\frac{\partial f}{\partial q} \tag{11}$$

and

$$H = \frac{\partial f}{\partial p_m'}\left(\frac{\partial p_m'}{\partial \varepsilon_v^p}\frac{\partial g}{\partial p'} + \frac{\partial p_m'}{\partial \varepsilon_q^p}\frac{\partial g}{\partial q}\right) \tag{12}$$

The plasticity properties used in this study were summarized in Table 3. In this study, λ and κ were calculated for weathered soil (sample used in test), and M used the results of the triaxial tests. D and β are parameters for the test, and the test was performed by calibration of the input parameters using trial and error methods.

4. Numerical simulation of the behavior of test soil under monotonic shearing

Figs. 4 and 5 were conventional CIU triaxial testing results done on moist tamped samples at loose (30%) and dense (70%) relative density and three different initial mean effective stresses of about 50, 100, and 300 kPa respectively. The dotted lines in Figs. 4 and 5 show the stress path, stress strain curve, excess pore pressure and M value respectively at different relative densities in these tests.

The experimental results were simulated using the stress strain relation given in Eq. (10). The model was written in python programming language to simulate a single element test.

The results of these numerical simulations are superimposed as continuous line in the same plots as experimental results. The continuous lines in Figs. 4 and 5

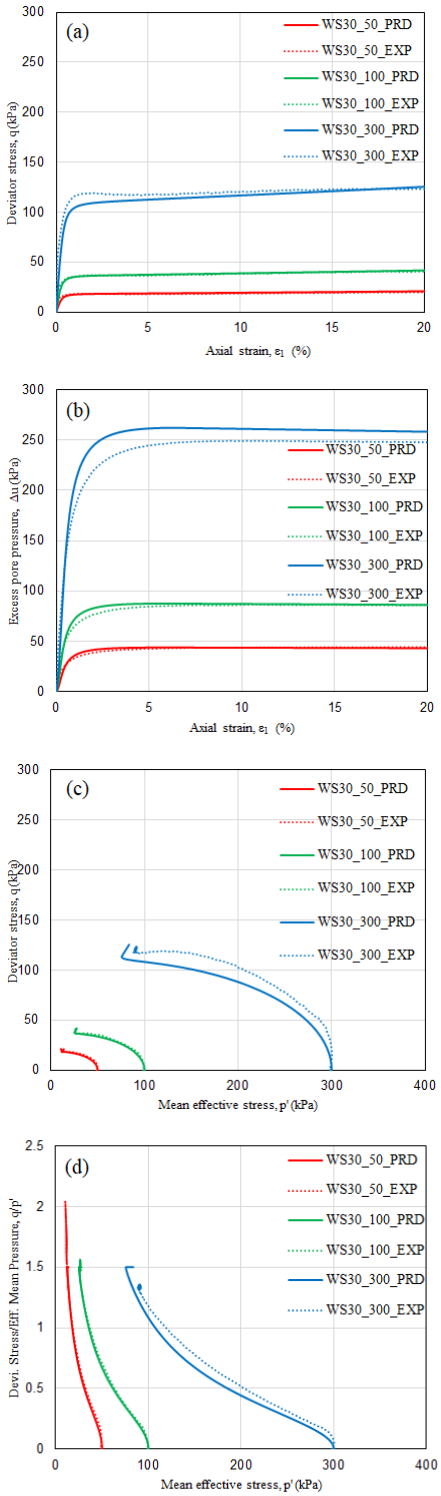

Fig. 4 Comparison of predicted values with experimental data (relative density = 30%)

show the stress path, stress strain curve, excess pore pressure and M value respectively at loose (30%) and dense (70%) relative density in these tests. The parameters used in these tests are given in Table 3. Parameters λ and κ were obtained from triaxial consolidation and swelling tests as the slope of the normal compression line and unloading reloading line in compression space. Parameter M was

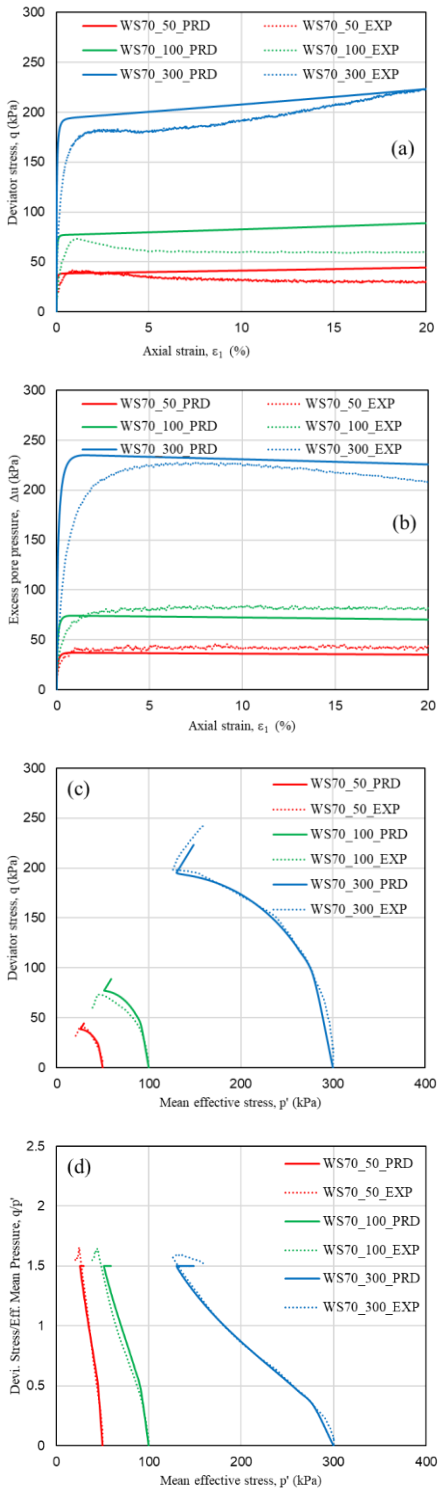

Fig. 5 Comparison of predicted values with experimental data (relative density = 70%)

obtained as the slope of the CSL in stress space. Parameter β and D were parametrically obtained to match the soil behavior. These parameters are depended on the soil particle arrangement and densities.

Comparing the stress strain curves in experimental and numerical simulation in Figs. 4(a) and 5(a), very close prediction is obtained suing the numerical simulations. The

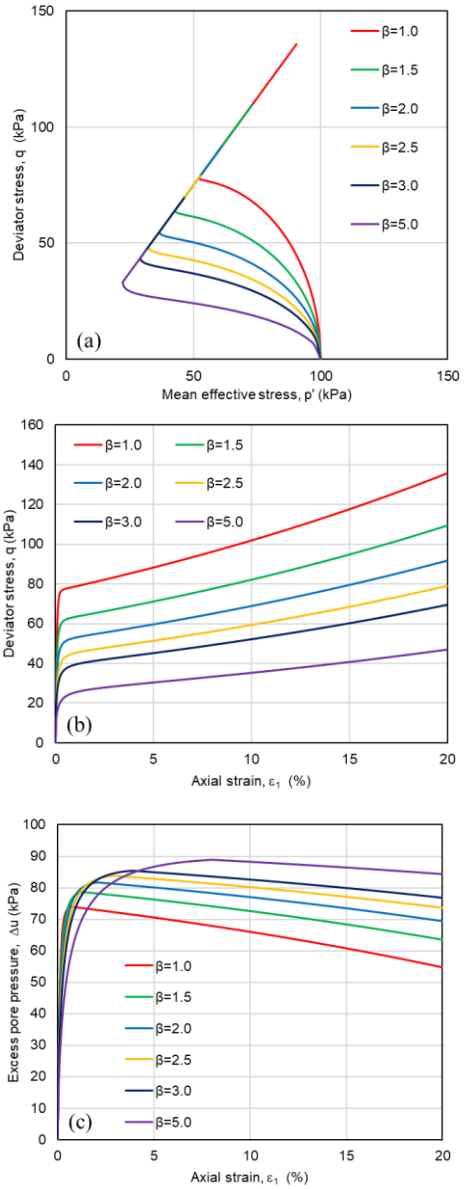

Fig. 6 The effect of different values of β

model is able to closely follow the initial high stiffness portion, and the later shear hardening. A comparison of the excess pore pressure in experimental and numerical simulation in Figs. 4(b) and 5(b) shows the model is able to predict the changes in effective stress quite well. The stress paths in Figs. 4(c) and 5(c) show that the model is able to follow the elliptical initial path and the deviator hardening shown by the soil. It can be seen that the stress paths in Figs. 4(d) and 5(d) correspond to the predicted parameter M again after compression and expansion in the case of the experimental values.

5. Parametric study

To study the effect of parameters β and D, a parametric study was done by suing a range of β and D respectively and holding other parameters constant.

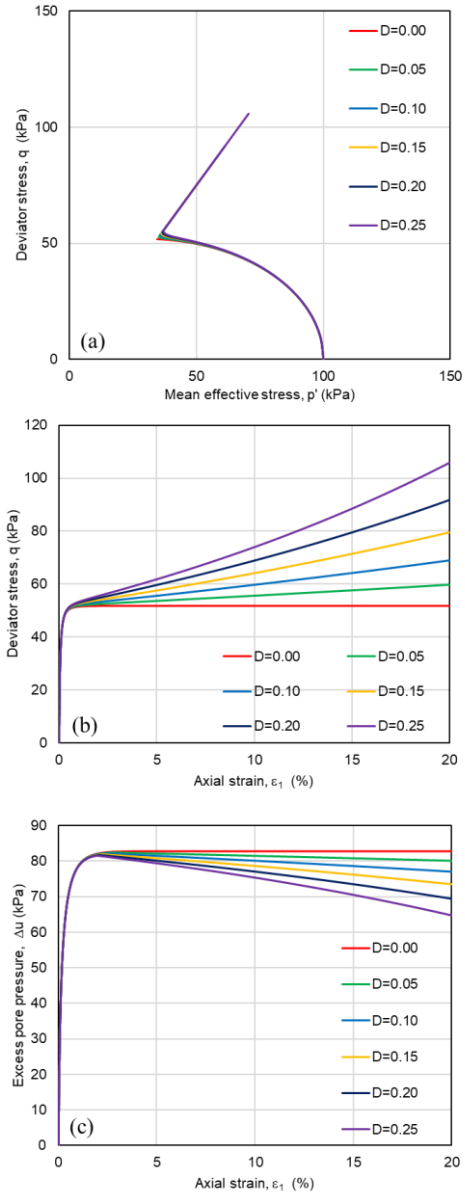

Fig. 7 The effect of different values of D

5.1 Effect of β

Parameter β controls the aspect ratio of the ellipse and hence also decides the deviator stress at the phase transformation state. From Fig. 6, it can be clearly seen that higher the values of β lower is the phase transformation deviator stress and also lower is the strength of the soil. From Fig. 6, it can be seen that for higher β values phase transformation happens at much higher strains.

5.2 Effect of D

Parameter D controls the deviator shear hardening in the soil and strongly influences the post phase transformation rate of strength gain. This can be seen from Fig. 7. A D value of zero may be used when no shear hardening in expected in the soil. From the calibration of the model for the undrained behavior of Korean weathered silty sand made under different sample preparation methods at different densities and effective stress, it is seen that parameters β and D are decided by the soil preparation method and densities.

By using parameters β and D, the model developed in this study can simulate the 4 types of undrained triaxial behavior reported by Castro (1969); and Yoshimine *et al.* (1998) (Fig. 7). it has been known that the sand behavior during undrained monotonic loading can be categorized into two different types due to the dilative and contractive nature of sand of loose and dense conditions.

6. Conclusions

The behavior of a typical weathered SM soil has been investigated in the laboratory under triaxial loadings. The isotropically consolidated samples were tested in the triaxial testing device under monotonic undrained loading. The test results were analyzed and their behaviors were interpreted within the framework of plasticity constitutive model for a weathered Korean silty sand. Possible physical bases for the proposed forms are discussed. Validation of the applied model using the laboratory results is also given. The proposed plasticity constitutive model for this soil was adopted to describe the soil behavior and able to predict closely the test soils. Based on this, the following conclusions were drawn:

(1) There exist failure line $q/p' = M_c$ that is independent of the confining pressure and relative density for the tested range ($p_o \leq 300$ kPa).
(2) There also exist the phase transformation(dilation) lines for triaxial compression in the p-q space for test SM soils with relative density loose (30%) and dense (70%).

The constitutive relationships for the weathered SM soil in undrained triaxial loading can be derived and treated by equation (10) with a proper constraint on the strain rate, $\varepsilon_v = 0$. It is shown the reliable adaptability of the constitutive model to weathered soils.

Data availability statement

The experimental data discussed in the manuscript are covered in Figures. If any further experimental data that support the findings of this study are required, they can be furnished by the author upon request.

Acknowledgments

This work was supported by a Basic Science Research Program through the National Research Foundation of Korea (NRF) funded by the Ministry of Education (No. 2018R1A6A1A08025348).

References

Abdul-Khader, M.-A. and Jeong, S. (2021), "Behavior of weathered soil under combined undrained cyclic-monotonic loading", *Int. J. Geomech.*, **21**, 04021026. https://doi.org/10.1061/(ASCE)GM.1943-5622.0001969.

Aziz, M. (2020), "Using grain size to predict engineering properties of natural sands in Pakistan", *Geomech. Eng.*, **22**(2), 165-171. https://doi.org/10.12989/gae.2009.1.4.263.

Beaty, M. and Byrne, P.M. (1998), "An effective stress model for predicting liquefaction behaviour of sand", *Proceedings of the Specialty Conference,* Seattle, WA, USA, August.

Castro, G. (1969), "Liquefaction of sands", *Harvard Soil Mechanics Series*, **81**, Cambridge, Massachusetts.

Dafalias, Y.F. and Manzari, M.T. (2004), "Simple plasticity sand model accounting for fabric change effects", *J. Eng. Mech.,* **130**, 622–634. https://doi.org/10.1061/(ASCE)0733-9399(2004)130:6(622).

Fleming, L.N. and Duncan, J.M. (1990), "Stress-deformation characteristics of Alaskan silt", *J. Geotech. Eng*., **116**, 377-393. https://doi.org/10.1061/(ASCE)0733-9410(1990)116:3(377).

Geocomp Corp. (2013), *Lab Services: Soil Testing*, Geocomp Corp., Acton, MA, USA.

Georgiannou, V.N., Burland, J.B. and Hight, D.W. (1990), "The undrained behaviour of clayey sands in triaxial compression and extension", *Géotechnique*, **40**, 431-449.

Gu, R., Fang, Y., Jiang, Q. and Li, B. (2022), "Effect of particle size on direct shear deformation of soil", *Geomech. Eng.,* **28**(2), 135-143. https://doi.org/10.12989/gae.2022.28.2.135.

Jefferies, M.G. (1993), "Nor-sand: a simple critical state model for sand", *Géotechnique*, **43**(1), 91-103.

Lee, S.G. and de Freitas, M.H. (1989), "A revision of the description and classification of weathered granite and its application to granites in Korea", *Q. J. Eng. Geol.*, **22**(1), 31-48. https://doi.org/10.1144/GSL.QJEG.1989.022.01.0.

Li, C. and Zoua, J.F. (2019), "Created cavity expansion solution in anisotropic and drained condition based on Cam-Clay model", *Geomech. Eng.,* **19**(2), 141-151. https://doi.org/10.12989/gae.2019.19.2.141.

Lin, H.D., Wang, C.C. and Wang, X.H. (2018), "A simplified method to estimate the total cohesion of unsaturated soil using an UC test", *Geomech. Eng.,* **16**(6), 599-608. https://doi.org/10.12989/gae.2018. 16.6.599.

Nova, R. and Wood, D.M. (1979), "A constitutive model for sand in triaxial compression", *Int. J. Numer. Anal. Method. Geomech.,* **3**, 255-278. https://doi.org/10.1002/nag.1610030305.

Peters, J.F. (1988), "Determination of undrained shear strength of low plasticity clays", *Proceedings of the Symposium on Advanced Triaxial Testing of Soil and Rock. Louisville*, KY, USA, June.

Puebla, H., Byrne, P.M. and Phillips, R. (1997), "Analysis of CANLEX liquefaction embankments: prototype and centrifuge models", *Can. Geotech. J.*, **34**, 641=657. https://doi.org/10.1139/t97-034.

Roscoe, K. and Burland, J.B. (1968), "On the generalized stress-strain behaviour of wet clay", *Engineering Plasticity*, Cambridge University Press, Cambridge, 535-609.

Shin, J.H. and Jeong, S.S. (1999), "Undrained Behavior of Clay-Sand Mixtures under Triaxial Loading", *J. Korean Geotech. Soc.*, **15**(3), 71-81.

Silvestri, V. and Abou-Samra, G. (2012), "Analytical solution for undrained plane strain expansion of a cylindrical cavity in modified cam clay", *Geomech. Eng.,* **4**(1), 19-37. https://doi.org/10.12989/gae.2009.1.4.263.

Wood, D.M. (1990), *Soil behaviour and critical state soil mechanics*. Cambridge university press, Cambridge, UK.

Yoshimine, M., Ishihara, K. and Vargas, W. (1998), "Effects of principal stress direction and intermediate principal stress on undrained shear behavior of sand", *Soils Found.*, **38**(3), 179-188.

Yu, Y. and Axelsson, K. (1992), "A Plasticity Model for Silt", *Proceedings of the Fourth International Symposium on Numerical Models in Geomechanics*, Swansea, UK, August.

Ziotopoulou, K. and Boulanger, R.W. (2013), "Numerical modeling issues in predicting post-liquefaction reconsolidation strains and settlements", *Proceedings of The 10th International Conference on Urban Earthquake Engineering*, Tokyo, Japan, March.

GC